Hydrodynamic interaction loads on a cylinder at acute free-surface angle

Ignacio Johannesen, Fabio Pierella and Henrik Bredmose
DTU Wind and Energy Systems, Kgs. Lyngby, Denmark
iapjo@dtu.dk

1 Introduction

Surface piercing inclined cylinders are a common element of offshore structures. For Floating Wind Turbines (FWT), these are subject nonlinear forces from waves and motion, together with nonlinear interaction forces from the combination of the two. Here, quadratic and cubic interaction forces of an inclined cylinder are addressed experimentally. Quadratic and cubic interaction forces are isolated by an extension of the harmonic separation methodology. We next compare the results against a Rainey based force model [1], that includes wave-wave and motion-wave quadratic forces.

2 Experimental campaign

The experimental campaign was conducted in the deep-water basin at DHI Denmark, see figure 1. Stochastic wave trains were propagated in the direction of the cylinder's longitudinal axis, while a stochastic rotational motion around its downstream end point was applied by an electric actuator.

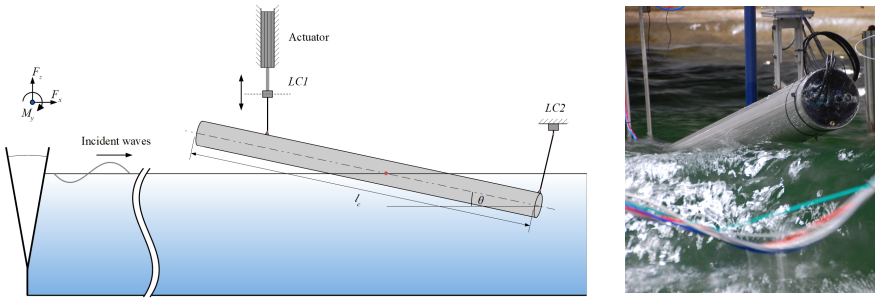

Figure 1: Experimental setup sketch with main parameters and real setup picture.

The cylindrical model was 2.8 m and 0.204 m, in length (L) and diameter (D). It was suspended by two supporting arms equipped with load cells (LC). The forced oscillatory motion was derived from a previous experimental campaign on a TetraSpar FWT design variant [2], representing the motion response to the applied sea state ($H_s = 0.218$ [m] and $T_p = 2.245$ [s]).

3 Analysis of experimental data

To isolate the non-linear forces and specifically the ones from interaction origin, the harmonic separation technique [3] is used, extended with motion. The tests were carried out as eight realizations, with the following combinations of positive and negative phase for the wave and motion input.

Waves and Motion	A	B	C	D	E	F	G	H
Waves	+	-			+	+	-	-
Motion			+	-	+	-	+	-

This approach is slightly different to the one of [4], where all tests included both waves and motion and a larger set of phase angles was applied. To isolate the motion-wave interaction loads, we first subtracted the wave-only and motion-only test results from the combined tests (E–H), for

instance $E' = E - A - C$. Next, we derived expressions for the isolated interaction forces, where three of them can be stated as

$$F^{(\eta^{(1)})} = \frac{A+B}{2} \quad , \quad F_{int}^{(\eta^{(1)}\xi^{(1)})} = \frac{E' - F' - G' + H'}{4} \quad , \quad F_{int}^{(\eta^{(2)}\xi^{(1)})} = \frac{E' - F' + G' - H'}{4} \tag{1}$$

The first of these, the odd harmonic wave excitation force is well known, while the present isolation of the quadratic interaction force and the cubic wave-wave-motion force is novel. While (1) allows to separate long time series of the isolated terms, physical insight can be obtained by conditional averaging. This is presented in figure 2. For each of the forces in (1), the 40 highest peaks were selected, and plotted along with their averaged signal in the top panels. The rows below present conditioned signals and averages for the wave and structural position, cropped and averaged by the same time windows as for the upper row.

In column 1 it can be seen that the averaged highest events of $F^{(\eta^{(1)})}$ resembles a NewWave group structure, where in contrast to monopiles, the main force peak is roughly in phase with the wave. This can be understood as that this force, mostly linear, is dominated by Froude-krylov forces, from the dynamic pressure effect on the (almost) vertical cylinder normal, which is in phase with the wave. The small misalignment between the peaks, might come from the difference on where the wave is measured and the action point of the developed force on the cylinder.

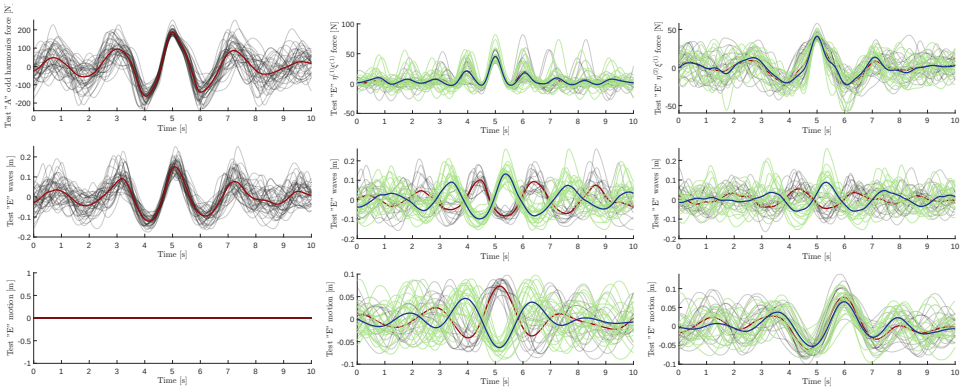

Figure 2: Experimental analysis using averaging methodology, for the odd harmonic wave only force (left), quadratic interaction force (mid) and one of the cubic interaction forces (right).

The middle column shows the first nonlinear interaction force ($\eta^{(1)}\xi^{(1)}$). The averaged signal has a frequency that correspond to the double of the wave and the first order forcing, which is expected. The conditioned wave and motion signals, present a pattern that can be grouped into two pairs. Either, positive wave crest at maximum draft or wave trough with minimum draft. Given the quadratic nature of the force, it makes sense that positive peaks can be obtained by a sign shift in both signals. The mechanism behind a 'green' large quadratic force peak can be seen as a maximization of the linear wave force through deep submergence, while the 'red' peaks are obtained by minimizing the negative linear force under a trough by small submergence.

The last column of figure 2, present the first of the two possible third harmonic interaction forces, $\eta^{(2)}\xi^{(1)}$ and $\eta^{(1)}\xi^{(2)}$. Here, two groups are also identified, related to a the wave crest or trough, while occurring when the cylinder is submerged the most. A possible explanation is that this forcing mechanism can maximizes the fixed body quadratic wave-wave loading. This force (not shown here) which has a peak close to the wave crest and trough. Hence, deep submersion will enhance this force and lead to an averaged peak in $F_{int}^{(\eta^{(2)}\xi^{(1)})}$.

4 Force model

A force model is defined based on Rainey's [1] slender-body theory with added drag. The total

force on the cylinder consists of the inertial forces from the structural acceleration and buoyancy (F_I, F_B) and the intersection load with the free surface F_R. Further, there is a force at the cylinder bottom F_E and a distributed force along its wetted length:

$$F_T(t) = F_I(t) + F_B(t) + F_R(t) + F_E(t) + \int_{s=0}^{s=l_{w0}(t)} \underline{df}(t) ds \tag{2}$$

The distributed $\underline{df}$ along the cylinder axis s is given by

$$\begin{aligned} \underline{df}(t) = &-M'(\ddot{\underline{\xi}} \cdot \underline{n})\underline{n} + M'_m(\dot{\underline{u}} \cdot \underline{n})\underline{n} + M'(\mathbf{V}l \cdot l)((\underline{u} - \dot{\underline{\xi}}) \cdot \underline{n})\underline{n} \\ &-2M'(\underline{\omega} \times \underline{l})(\underline{u} \cdot \underline{l}) + \frac{1}{2}\rho C_d D[(\underline{u} - \dot{\underline{\xi}}) \cdot \underline{n}]|(\underline{u} - \dot{\underline{\xi}}) \cdot \underline{n}|\underline{n} \end{aligned} \tag{3}$$

where $\underline{u}$ is the fluid velocity, M' the added mass, $\mathbf{V}$ the velocity gradient matrix, C_d the drag coefficient and D the cylinder diameter. The inclination angle $\theta(t)$, defines the instantaneous normal to the cylinders axis $\underline{n}$, the rotation speed ω and the local structural position $\underline{\xi}$.

While (2)–(3) can be evaluated for each time step in the instantaneous structural location we chose to expand from the mean body position and develop a force model with explicit quadratic wave-wave and motion-wave force terms. This offers insight for the role of each term and increases the numerical efficiency. We thus expand θ as $\theta = \theta_0 + \delta\theta$ and retain all terms of order $\eta^{(1)}\eta^{(1)}$ and $\eta^{(1)}\delta\theta$. Hereby, the integration along the body is split into integration along its mean wetted length plus a second-order point force with both wave-wave and motion-wave terms

$$F_{l'_w} = l'_w \left[\rho\frac{\pi}{4}D^2(C_a + 1)\left[(\underline{u}_t \cdot \underline{n_0})\underline{n_0}\right]\right] \quad , \quad l'_w = \left(\frac{\eta}{\sin(\theta_0)} - \frac{\delta\theta\, d\cos(\theta_0)}{\sin(\theta_0)^2}\right) \tag{4}$$

Further motion-wave terms (not shown here) arise from (3), from the change in normal vector direction, drag and change in position. Through analysis of the test results, we found that the acute angle and thus large water plane area A_w required to add an explicit representation of the Froude Krylov force for the intersection zone

$$F^{(1)}_{FKw} = A_w P_{dyn} \quad , \quad F^{(2)}_{FKw} = \frac{\eta}{sin(\theta_0)}\frac{\partial}{\partial\eta}P_{dyn} - \frac{\delta\theta dcos(\theta_0)}{sin(\theta_0)^2}\frac{\partial}{\partial\theta}P_{dyn} \tag{5}$$

where p_{dyn} is the dynamic pressure with a corresponding added mass force not shown here. The linear force was checked against radiation-diffraction theory.

5 Force Model Analysis

With the force model defined, the same results from figure 2 are calculated, following the same steps and methodologies, but using simulated results for all the eight experimental realizations. Twenty points was used for the conditioning analysis.

In the first column of figure 3, we observe a similar behaviour and magnitude to the experimental result in figure 2, on the wave-only force. The force, however, resembles a more linear response than the experimental averaged force. This can be expected since the force model is truncated at second order, and therefore, only the linear response will fall into the odd harmonics. The conditioned wave signal behaves similarly to the experimental, however, present larger scattering. These differences on the averaged wave can be related to the wave 'measuring point'. Experimentally, it lies at the free-surface piercing centre, while numerically at the cylinder's submerged end.

The second column shows the quadratic interaction force $F^{\eta^{(1)}\xi^{(1)}}$. The averaged signals is similar to the experimental of figure 2 with resembling grouping and phasing of the conditioned

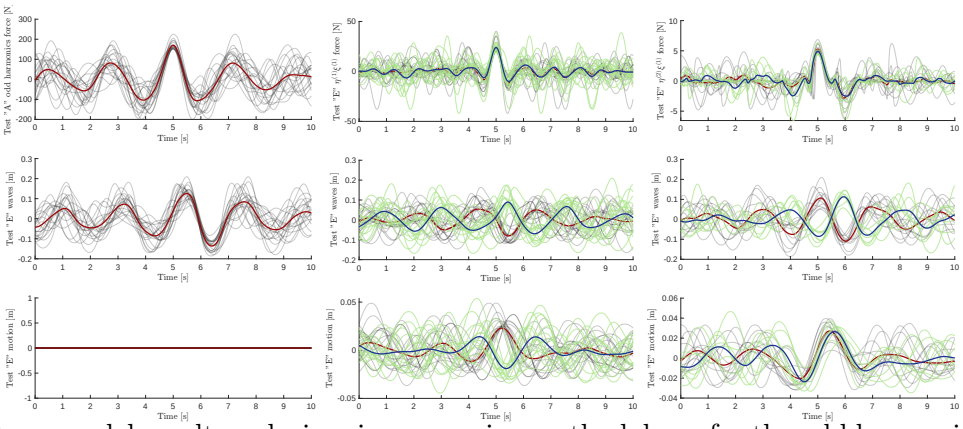

Figure 3: Force model result analysis using averaging methodology, for the odd harmonic wave only force, the quadratic interaction force and one of the cubic interaction terms.

signals. The magnitude of the force peak, though, is ($\approx -30\%$) smaller than the experimental one. Possible reasons for this includes the choice of force coefficients ($C_a = C_d = 1$) and the simplicity of the force model, where the assumption of slender-body and small deviations from the mean body position might break down in the free surface region, owing to the cylinder's acute inclination angle.

The last column shows the cubic force $F^{(\eta^{(2)}\xi^{(1)})}$, which is not directly part of the model. However, it is known that when separating the Stokes-like harmonics, the drag loads can fall into the odd harmonics of cubic order, as investigated in [5]. This is also the case for the present model, since the motion-relative drag term will produce force components of type $|u|\dot{\xi}$ which will be grouped into the $F^{(\eta^{(2)}\xi^{(1)})}$ terms. Accordingly, the resulting conditioned numerical force resembles the shape of drag forcing with its peak occurring when waves are around the zero crossing, while being fully submerged. In comparison to the experimental results, the magnitude is significantly smaller ($\approx 20\%$ of magnitude), showing that the experimental force is not fully dominated by this mechanism. However, it is interesting to see that the wave and motion behaviour agrees with what is observed in figure 2, suggesting that at least in part it is a relevant force contribution that can coexist with other third harmonic and cubic forcing mechanisms.

The present results are encouraging, given the acute angle of the cylinder that distributes the resulting loads across a large horizontal stretch and challenges the slender-body assumption. Our ongoing work includes analysis of the $F^{(\eta^{(1)}\xi^{(2)})}$ term and deeper comparison to individual terms in the force model.

This research was supported by FloatLab (grant no 2079-00082B) project funded by Innovation Fund Denmark.

REFERENCES

[1] Rainey, R. The hydrodynamic load at the intersection of a cylinder with the water surface. In *Proceedings of 10th International Workshop on Water Waves and Floating Bodies* (1995), pp. 207–210.

[2] Borg, M., Pegalajar-Jurado, A., Stiesdal, H., Madsen, F., Nielsen, T., Mikkelsen, R., Mirzaei, M., Lomholt, A., and Bredmose, H. 2024. *Dynamic response analysis of the TetraSpar floater in waves: Experiment and numerical reproduction. Marine Structures 94*, 103546.

[3] Jonathan, P., and Taylor, P. H. 1997. *On irregular, nonlinear waves in a spread sea.*

[4] Wolgamot, H., Orszaghova, J., Kurniawan, A., Taylor, P., and Todalshaug, J. H. Phase-manipulation with multiple controlled inputs to enhance investigation of nonlinear hydrodynamic effects. In *38th International Workshop on Water Waves and Floating Bodies* (2023).

[5] Orszaghova, J., Taylor, P. H., Wolgamot, H. A., Madsen, F. J., Pegalajar-Jurado, A. M., and Bredmose, H. 2021. *Wave-and drag-driven subharmonic responses of a floating wind turbine. Journal of Fluid Mechanics 929*, A32.